TRANSNAV
http://www.transnav.eu
the International Journal
on Marine Navigation
and Safety of Sea Transportation
Volume 19
Number 2
June 2025
DOI: 10.12716/1001.19.02.27

CFD Analysis of Cobalt-Based Ceramic Coatings for Energy Optimization in the Fishing Naval Industry

D.S. Sanz[1], S. García[1], J. García[1], D. Boullosa-Falces[2] & A. Trueba[1]
[1] *University of Cantabria, Santander, Spain*
[2] *University of the Basque Country, Portugalete, Spain*

ABSTRACT: The rising cost of fossil fuels has created a significant economic challenge for the fishing fleet, whose performance heavily relies on marine diesel consumption. The increase in operational costs due to fuel price surges negatively impacts the profitability of ships, particularly in the fishing industry, where profit margins are often tight. Given this issue, it is crucial to explore solutions that reduce fuel consumption without compromising the operational efficiency of ships. In this context, cobalt-based ceramic coatings, designed and tested in accordance with the ASTM-D3623 procedure, emerge as an innovative and promising alternative. These coatings reduce biofouling adhesion, a buildup of marine organisms on the ship's hull that increases frictional resistance to movement, consequently leading to higher fuel consumption. By decreasing hydrodynamic resistance, ships require less energy for propulsion, thereby optimizing fuel consumption. Additionally, these coatings provide anticorrosive protection, extending the service life of ships and reducing maintenance costs. The cobalt-based coating has been tested under controlled laboratory conditions and subjected to hydrodynamic shear forces representative of ship navigation at a speed of 10 knots. This article evaluates via CFD the impact of these coatings on the drag resistance of a trawler ship, demonstrating that the increase in hull roughness due to biofouling adhesion on the cobalt-based ceramic coating after one month of navigation results in a 0.02% increase in drag. In contrast, the Intersleek 1001 coating leads to a 6.35% increase in drag under the same conditions.

1 INTRODUCTION

One of the principal challenges in global fisheries is advancing sustainable fishing practices that minimize environmental degradation while enhancing societal advantages One of the most significant environmental concerns is the high level of fuel consumption in capture fisheries, which contributes to greenhouse gas emissions. Many countries subsidize fuel, further complicating efforts to curb emissions. Given the economic reliance on fuel in the fishing industry, finding fuel-efficient methods for seafood production has been a long-standing priority. Over the years, various technical innovations have been introduced, such as modernizing fishing fleets, investing in energy-efficient propellers and gears, replacing engines, and improving vessel hull designs [1–3].

The design of a ship's hull plays a crucial role in hydrodynamics, stability, safety, and operational efficiency. However, additional variables, including hull biofouling, can modify the topographical characteristics of the hull surface, leading to increased hydrodynamic drag and elevated fuel expenditure [4,5].

To address these challenges, regulatory bodies like the International Maritime Organization (IMO) have implemented strict energy efficiency measures. The 2014 amendment to MARPOL ANNEX IV introduced the Energy Efficiency Design Index (EEDI) for new ships and the Ship Energy Efficiency Management Plan (SEEMP) for existing vessels. Moreover, IMO has set ambitious targets, aiming for a 40% reduction in CO2 emissions by 2030 and a 70% reduction by 2050 compared to 2008 levels. These regulations push the shipping industry to optimize vessel efficiency and minimize environmental impact [6].

Computational Fluid Dynamics (CFD) has become an essential tool for improving ship hull design, allowing researchers to simulate hydrodynamic conditions and predict the impact of hull roughness and biofouling on frictional resistance. Several studies have demonstrated CFD's effectiveness in this area. [7] employed roughness functions in CFD simulations, though they did not incorporate Reynolds-averaged Navier-Stokes (RANS) calculations, which are crucial for accurately modelling turbulent flows. Izaguirre-Alza et al. used Star-CCM+ software to validate surface roughness effects but relied on built-in roughness functions [8].

Recent CFD advancements have aimed at improving predictive accuracy. [9] introduced a CFD model incorporating fouling control coatings, validating results against experimental data. Later, they applied a RANS model with a modified roughness function to predict efficiency losses due to hull deterioration. Other researchers, such as [10,11], analysed biofouling effects on propeller efficiency, while [12] developed a methodology using OpenFOAM to estimate frictional resistance.

As the shipping industry seeks energy-efficient solutions to comply with environmental regulations, advanced CFD models will play a key role in optimizing hull design, reducing fuel consumption, and minimizing greenhouse gas emissions [1].

Biofouling refers to the unwanted adhesion and accumulation of biotic deposits on surfaces submerged in seawater [13–15]. These deposits primarily consist of organic biofilms formed by microorganisms embedded in a self-produced polymeric matrix, which can also trap inorganic particles such as salts or corrosion by products [16]. Over time, microbial biofouling facilitates the settlement of larger macro-organisms, leading to macro-fouling. This phenomenon presents a significant challenge to various sectors of the blue economy, particularly maritime transportation, where biofouling can increase hydrodynamic drag, reducing ship performance and elevating fuel consumption by up to 30% to maintain operational efficiency. The subsequent rise in fuel demand has both economic and environmental consequences, as fuel costs account for nearly 50% of marine transportation expenses and increased combustion results in higher greenhouse gas emissions [17].

To mitigate the adverse effects of biofouling in fishing vessels, marine antifouling coatings have been developed to inhibit biofouling growth either by releasing active biocidal agents or by providing a smooth, non-stick surface that prevents the settlement of fouling organisms. These coatings significantly reduce frictional resistance, thereby improving vessel efficiency, lowering fuel consumption, and decreasing greenhouse gas emissions. Given the high dependency of fishing fleets on fuel, enhancing hydrodynamic efficiency is crucial for achieving more sustainable and cost-effective operations. However, different fouling control coatings vary in surface roughness and durability, influencing their effectiveness in minimizing frictional resistance over time. Hence, accurately assessing the impact of different coatings on vessel performance is essential for optimizing their application in the fishing industry. Studies suggest that full-scale ship resistance and power requirements for various antifouling coatings can be predicted using laboratory drag measurements and boundary layer similarity laws. Moreover, empirical correlations have been established to estimate frictional resistance in different fouling conditions, providing valuable insights for coating selection and maintenance strategies [18].

Biofouling and corrosion, though distinct processes, often coexist and exacerbate material degradation in marine environments, particularly in fishing vessels that operate under diverse oceanographic conditions. Biofouling involves the colonization of submerged surfaces by microorganisms such as bacteria and algae, which form biofilms that serve as substrates for larger fouling organisms like barnacles and mussels [19]. The development of biofilms is influenced by multiple factors, including water temperature, nutrient availability, flow dynamics, and surface composition. Smooth, defect-free surfaces generally exhibit lower biofouling susceptibility compared to rough or irregular surfaces. Furthermore, nutrient-rich waters encountered in fishing grounds facilitate microbial proliferation, enhancing biofilm growth and subsequent macro-fouling, which significantly affects vessel performance by increasing drag and fuel consumption [20].

Corrosion, on the other hand, is the deterioration of materials through chemical or electrochemical reactions with their environment. In marine settings, saltwater exposure accelerates corrosion, leading to significant structural damage over time. Corrosion manifests in various forms, such as metal oxidation, steel degradation, and material fatigue, and is driven by factors including oxygen exposure, moisture, acidic conditions, and saline environments. The consequences of marine corrosion for fishing vessels include reduced hull integrity, increased maintenance costs, and potential safety hazards. For instance, corrosion-induced weakening of hull structures can elevate the risk of leaks, compromising vessel safety and operational efficiency. Therefore, corrosion prevention strategies are crucial for ensuring the longevity and reliability of fishing fleets. Common mitigation measures include the use of corrosion-resistant materials, protective coatings, and comprehensive corrosion monitoring systems [21]. The interaction between biofouling and corrosion is intricate, as biofouling can accelerate corrosion through microbial metabolic activity. Certain microorganisms produce acidic compounds that degrade material surfaces, while biofilms create microenvironments that promote localized corrosion. Additionally, biofouling can trap moisture and corrosion-inducing agents, further exacerbating material degradation. Consequently, integrated antifouling and anticorrosion strategies are essential for comprehensive fishing vessel maintenance. The development of advanced coatings that simultaneously provide antifouling and anticorrosion protection is a promising approach to mitigating these challenges and improving the sustainability of fishing operations [13,22,23].

Among these advanced coatings, cobalt-based enamels have demonstrated exceptional mechanical properties, including high resistance to erosion and corrosion [18]. Research has shown that these coatings exhibit high hardness and durability, making them highly effective in protecting fishing vessels against biofouling and material degradation. The surface of cobalt-based enamels is highly hydrophilic, preventing the adhesion of organic molecules—a critical initial step in biofilm formation. Additionally, the vitreous structure of ceramic glazes provides a smooth surface with an average roughness height of approximately 0.189 μm, reducing microbial adhesion and facilitating the removal of biofouling through hydrodynamic forces, thereby improving vessel efficiency and reducing fuel consumption.

One significant advantage of cobalt-based enamels is their environmental compatibility. Unlike traditional antifouling coatings that may contain toxic heavy metals such as copper, cobalt-based enamels do not release harmful substances into marine ecosystems. This environmentally friendly characteristic aligns with sustainability goals, making them a viable alternative for long-term applications in fishing fleets. Furthermore, these coatings exhibit remarkable durability, maintaining their protective properties even in highly corrosive marine environments, which is essential for vessels operating in harsh fishing grounds [24]. Biofouling and corrosion are major concerns for fishing vessels, impacting fuel efficiency, structural integrity, and environmental sustainability. The use of advanced antifouling and anticorrosion coatings, such as cobalt-based enamels, represents a promising solution for mitigating these challenges. Continued research and innovation in coating technology will play a pivotal role in enhancing the performance and longevity of fishing vessels while reducing operational costs and environmental impacts, contributing to the decarbonization of the fishing industry.

A Computational Fluid Dynamics (CFD)-based Reynolds Averaged Navier-Stokes (RANS) model was employed to analyse the hydrodynamic performance of a fishing vessel by modifying experimental variables. OpenFOAM (Open Field Operation and Manipulation), an open-source, C++-based software, was utilized due to its high accuracy in simulating rough hull conditions and its capability to integrate custom algorithms.

This study examined the impact of hull biofouling on surface roughness under both static and dynamic navigation conditions. Laboratory tests were conducted on a cobalt-based ceramic coating and a reference Intersleek 1001 coating to assess their performance. The experimentally obtained roughness data were then incorporated into the CFD model to evaluate the reduction in frictional resistance achieved through cobalt-based ceramic coatings. The findings demonstrate the potential of advanced coatings to enhance fuel efficiency and decrease greenhouse gas emissions in fishing vessels, contributing to the decarbonization of the fishing industry.

2 MATERIALS AND METHODS

2.1 *CFD simulations*

In this study, OpenFOAM is utilized as the primary Computational Fluid Dynamics (CFD) simulation tool. As an open-source C++ library, it adheres to an object-oriented programming paradigm and is distributed under a GPL license. OpenFOAM provides a wide range of solvers for simulating laminar and turbulent flows, single and multiphase systems, and adaptive meshing. Its modular architecture allows for extensive customization, making it particularly suitable for analyzing multi-phase turbulent flows involving floating bodies.

2.1.1 *Solver numerical model*

The hydrodynamic simulations in this study were performed using the interFoam solver in OpenFOAM, designed for incompressible, two-phase flow. The solver employs the Navier-Stokes Equation (1) and continuity equations Equation (2) to model laminar flow of Newtonian fluids.

$$\rho\left(\frac{\partial \upsilon}{\partial t}+\upsilon\cdot\nabla\upsilon\right)=-\nabla p+\mu\nabla^2\upsilon+\rho g \qquad (1)$$

$$\nabla\cdot\upsilon=0 \qquad (2)$$

Here, υ is the velocity, p is the pressure, ϱ is density, μ is the dynamic viscosity, g is the acceleration due to gravity and ∇2 is the Laplace operator.

Specifically, interFoam solves the Reynolds-Averaged Navier-Stokes (RANS) equations for two immiscible phases, air and water, using finite volume discretization and the Volume of Fluid (VOF) method to capture the free surface. The VOF method treats air and water as a single effective fluid, with the volume fraction of water (α) in each computational cell indicating the phase distribution: $\alpha = 1$ for water, $\alpha = 0$ for air, and $0 < \alpha < 1$ for mixed cells. The air-water interface is approximated by the iso-surface $\alpha = 0.5$. The local density (ϱ) and viscosity (μ) of the fluid, with μwater = 1.00E-3 Pa·s and μair = 1.48E-5 Pa·s, are determined for each computational cell using Equations (3) and (4).

$$\rho=\alpha\rho_{water}+\left(1-\alpha\right)\rho_{air} \qquad (3)$$

$$\mu=\alpha\mu_{water}+\left(1-\alpha\right)\mu_{air} \qquad (4)$$

2.1.2 *Fishing Vessels model, settings, and simulation mesh*

The hull model selected for this study corresponds to a factory trawler with a length between perpendicular of 48.17 meters, a beam of 12.00 meters, and a depth of 10.16 meters. It has a draft of 4.49 meters, a wetted surface area of 780.82 m^2, and a displacement volume of 1479.38 m^3 (Table 1). Las formas del modelo de buque se muestran en la Figure 1. The body plan of the ship model is presented in Figure 1.

Table 1. Full-scale trawler ship model specifications

Specification		Trawler ship
Length between perpendicular	Lpp (m)	48.17
Breadth	B (m)	12.00
Depth	D (m)	10.16
Draft	T (m)	4.49
Wetted surface area	S (m2)	780.82
Displacement volume	V (m3)	1479.38

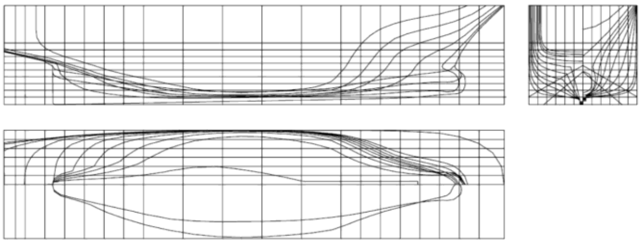

Figure 1. Body plan of the trawler ship model

In this study, the nutkRoughWallFunction model was implemented in OpenFOAM to account for surface roughness effects in viscous resistance predictions. Wall functions, derived from empirical equations, were applied to define near-wall boundary conditions for momentum and turbulence transport equations. The wall function model in OpenFOAM was based on the formulations proposed by [25] and [26]. To ensure the precise application of wall functions in mesh design, the y+ parameter, representing the non-dimensional boundary layer thickness, had to remain within a valid range. This constraint-imposed limitations on the size of the mesh cells adjacent to the hull surface, requiring their height to exceed the roughness value for proper recognition in the simulation.

The roughness model incorporated the sand-grain roughness height on the hull surface to improve the accuracy of viscous resistance predictions. Additionally, the roughness parameter influenced turbulence properties. The nutkRoughWallFunction boundary condition provided a turbulent kinematic viscosity definition to account for roughness effects, relying on turbulence kinetic energy.

OpenFOAM supported three turbulence models: k-ε, k-ω, and SST k-ω. In this study, turbulence was modeled using the Reynolds-Averaged Stress (RAS) SST k-ω two-equation model, with second-order upwind discretization applied to ensure numerical stability and accuracy.

To achieve accurate numerical simulation results, the mesh previously utilized in the investigations of [18] was adopted. The computational domain underwent five successive refinements in the vicinity of the hull to ensure adequate resolution, allowing for the precise capture of pressure and viscous forces. The snappyHexMesh utility was then employed to integrate the hull geometry into the simulation domain. This process included one additional refinement near the hull, two refinements directly on the hull surface, and the generation of boundary layers to maintain the required non-dimensional wall distance (y^+). The final mesh configuration, consisting of 6.95 million cells, resulted in a y^+ value of approximately 100. All simulations were conducted assuming a static hull, with no mesh motion or morphing applied.

2.1.3 *Frictional resistance calculation using CFD prediction*

The CFD model was employed to numerically predict viscous and pressure resistance, thereby determining the total drag along the X-axis for a navigation speed of 10 knots. To transform the experimentally obtained average roughness heights into equivalent sand-grain roughness heights, the conversion equation proposed by [27] (Equations (5)) was applied. The conversion equation used was:

$$k_s = 5.863 \cdot k_a \tag{5}$$

Here, k_s is the equivalent sand grain roughness height, and k_a is the average roughness height.

By incorporating Equation (5) into the CFD computational model, it was possible to avoid directly modeling the rough surface caused by biofouling, thereby reducing the computational effort required by the designer. This approach proved particularly advantageous when analyzing multiple roughness levels, as was the case in the present study. Moreover, accurately discretizing surface roughness would have necessitated a significantly refined mesh, leading to a considerable increase in computational cost and simulation time. This methodology was feasible because the correlation between the roughness function and the roughness Reynolds number was well established. Consequently, this correlation was incorporated into the OpenFOAM solver through the wall function and turbulence model, enabling an efficient and accurate representation of roughness effects.

CFD simulations were performed on a workstation equipped with a 13th Gen Intel® CoreTM i9-13900KF processor clocked at 3.00 GHz and 128 GB of installed RAM. For each simulation, 6 cores were employed.

2.2 *Experimental Phase*

2.2.1 *Preparation and composition of experimental panels*

The preparation of experimental steel panels coated with ceramic enamel followed a standardized multistep procedure to ensure optimal coating performance. The ceramic coating was applied to an S235JR steel panel measuring 150 × 400 mm with a thickness of 3 mm. Prior to the application of the ceramic coating, the steel surfaces underwent abrasive blast cleaning to achieve a surface roughness corresponding to grades Sa 2.5 or Sa 3 in accordance with ISO 8503. Surface cleanliness was ensured following ISO 8501 standards, and contamination levels were controlled so as not to exceed rating 2 as defined in ISO 8502-3. Subsequently, the application of a groundcoat layer was carried out

The enamel coating process consisted of sequential application of a primer (100 g/m²), groundcoat (450–500 g/m²), and covercoat (700–800 g/m²). Thermal treatment was carried out in a muffle furnace at 840 °C for the primer and groundcoat layers, and at 820 °C for the covercoat. Firing duration was adjusted according to substrate thickness to achieve proper sintering without compromising structural integrity. The enamel slurry was prepared using 100% TSSG00505/1 enamel frit combined with 40% water by weight. The mixture was homogenized for 10 minutes and sieved through a 60-mesh screen to ensure particle size uniformity. The final slurry exhibited a specific gravity in the range of 1.75–1.77 g/ml, suitable for achieving consistent coating thickness.

The qualitative chemical composition of the enamel included more than 30% SiO_2 as the primary glass-forming oxide. Additionally, 5–15% of Na_2O and B_2O_3 acted as fluxing agents, while minor constituents (<5%) such as Li_2O, K_2O, CaO, MnO, CoO, CuO, Al_2O_3, TiO_2, ZrO_2, and F provided specific functional and structural properties to the final enamel layer.

2.2.2 *Static and Dynamic Testing*

The experimental test was conducted in accordance with ASTM D4939-89 at the Biofouling Laboratory of Cantabria University. This facility's strategic location allowed for the direct intake of seawater from the Bay of Santander (43° 28′ N, 3° 48′ W) using a Grundfos SP 14-4R stainless steel submersible pump, which transported the water to the laboratory.

Throughout the experimental phase, a reference panel coated with the commercial antifouling paint Intersleek 1001 was evaluated in parallel with the cobalt-based ceramic coating. The test panels were fully immersed in seawater under static conditions (static test) inside an experimental reactor to facilitate biofouling development. These panels were mounted on a drum using plastic supports.

After a one-month static exposure, the dynamic test was initiated. This phase involved rotating the drum, where the test panels were mounted, at a speed of 10 knots. This setup was designed to replicate the hydrodynamic shear stress experienced on the hull of a fishing vessel during navigation (Figure 2).

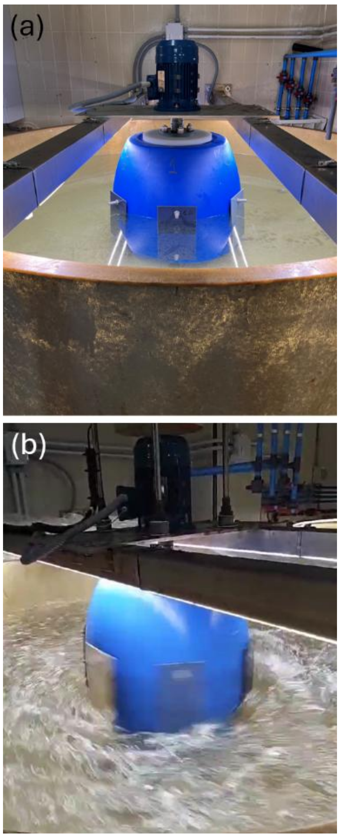

Figure 2. Experimental reactor: (a) static test, (b) Dynamic test.

2.2.3 *Surface Roughness Characterization of Ceramic Coating*

The surface roughness of the cobalt-based ceramic coating was measured three times throughout the experimental phase, following the guidelines established in ASME/ANSI B46.1-2009. The first measurement was taken prior to experimentation, the second after one month of seawater immersion in the reactor (static test), and the third following a one-month dynamic test. The initial roughness characterization of both the ceramic coating and the Intersleek 1001 marine paint was carried out using a contact profilometer (Taylor-Hobson, Surtronic 3+). After the static and dynamic exposures, when the surfaces were covered with biofouling, roughness measurements were performed using the TQC surface roughness tester (DC9000 Series), which is accurate to ±5 microns or <2%.

3 RESULTS AND DISCUSION

3.1 *Experimental study*

The results obtained during the experimental phase are presented in Table 2. Before exposure in sea water, the cobalt-based ceramic coating exhibited significantly lower roughness values (Ka = 0.25 μm, Ks = 1.44 μm) compared to Intersleek 1001 (Ka = 5.12 μm, Ks = 30.02 μm), representing a 1948.0% higher roughness for Intersleek 1001.

After 30 days of static seawater exposure, both coatings experienced an increase in roughness due to biofouling accumulation. The cobalt-based coating reached Ka = 10.21 μm and Ks = 59.86 μm, whereas Intersleek 1001 showed lower roughness values (Ka = 7.83 μm, Ks = 45.91 μm), indicating 23.31% less biofouling adhesion compared to the ceramic coating. The roughness data obtained for the cobalt-based ceramic coating exhibited highly similar values compared to those reported by [4,5] in his studies on a coating with similar characteristics, showing a roughness variation of only 1.47%.

Under dynamic conditions, after 30 days of exposure simulating navigation at 10 knots, the roughness of the cobalt-based ceramic coating significantly decreased (Ka = 0.31 μm, Ks = 1.82 μm), approaching its initial values. In contrast, the Intersleek 1001 coating maintained a higher roughness after the dynamic phase (Ka = 6.47 μm, Ks = 37.93 μm), suggesting a lower self-cleaning efficiency compared to the ceramic coating, un 1987.10% mas de rugosidad, with a 1987.10% higher roughness.

Table 2. Ceramic coatings roughness under different experimental conditions.

Condition	Coating	Ka μm	Ks μm
No exposure	Blue (Co)	0.25± 0.09	1.44±0.55
	Intersleek 1001	5.12± 1.24	30.02±7.27
30-days exposure	Blue (Co)	10.21±1.79	59.86±7.92
(Static Conditions)	Intersleek 1001	7,83±1.18	45.91±7.05
30-days exposure	Blue (Co)	0.31±0.10	1.82±0.32
(Dynamic Conditions)	Intersleek 1001	6.47±0.93	37.93±6.86

3.2 *CFD simulation at different fouling levels*

Each simulation required 50637.4 seconds of physical time to complete, producing a computational mesh of 7986487 cells, ensuring high-resolution domain discretization.

The CFD simulation results for a trawler hull model coated with the evaluated coatings under different exposure conditions are summarized in Table 3. Before seawater exposure, the hull coated with the cobalt-based ceramic exhibited a viscous resistance (Rv) of 1.47 kN and a total resistance (Rtot) of 5.45 kN. In contrast, the Intersleek 1001-coated hull showed slightly higher resistance values, with Rv = 1.50 kN and Rtot = 5.75 kN, representing a 5.58% increase in total resistance. Figure 3, 4 and 5 presents the results of the CFD simulation for the six different cases outlined in Table 3.

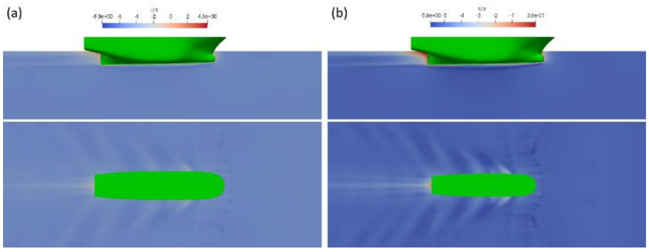

Figure 3. Velocity distribution on the hull surface under no-exposure condition: (a) Cobalt-based ceramic coating, (b) Intersleek 1001 coating.

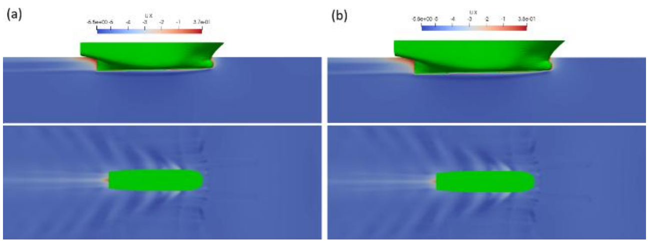

Figure 4. Velocity distribution on the hull surface under 30-days exposure in static conditions: (a) Cobalt-based ceramic coating, (b) Intersleek 1001 coating.

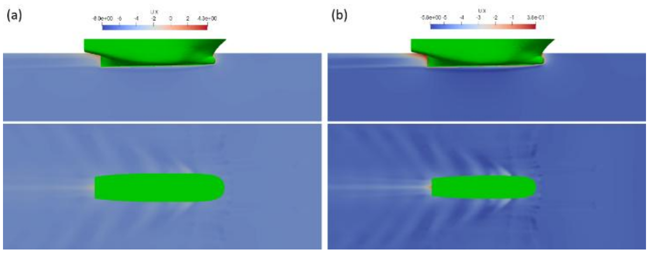

Figure 4. Velocity distribution on the hull surface under 30-days exposure in dynamic conditions: (a) Cobalt-based ceramic coating, (b) Intersleek 1001 coating.

After 30 days of static seawater exposure, biofouling accumulation led to an increase in hull resistance for both coatings. The trawler coated with the cobalt-based ceramic reached Rv = 1.73 kN and Rtot = 6.01 kN, reflecting a 10.40% rise in total resistance. The hull coated with Intersleek 1001 also experienced an increase, with Rv = 1.64 kN and Rtot = 5.89 kN, corresponding to an 8.09% increase in total resistance.

Under dynamic conditions, after 30 days of simulated navigation at 10 knots, the cobalt-based ceramic coating effectively restored its initial resistance values (Rv = 1.47 kN, Rtot = 5.45 kN), indicating successful biofouling removal and a negligible resistance variation of 0.02%. Conversely, the hull coated with Intersleek 1001 maintained higher resistance values (Rv = 1.51 kN, Rtot = 5.79 kN), leading to a 6.35% increase in total resistance, suggesting lower self-cleaning efficiency compared to the ceramic coating.

Table 3. Simulation results for ceramic and commercial coatings.

Condition	Coating	Viscous resistance R_v	Total resistance R_{tot}	Difference %
No exposure	Blue (Co)	1.47 E+04	5.45 E+04	0,00
	Intersleek 1001	1.50 E+04	5.75 E+04	5.58
30-days exposure	Blue (Co)	1.73 E+04	6.01 E+04	10.40
(Static Conditions)	Intersleek 1001	1.64 E+04	5.89 E+04	8.09
30-days exposure	Blue (Co)	1.47 E+04	5.45 E+04	0.02
(Dynamic Conditions)	Intersleek 1001	1.51 E+04	5.79 E+04	6.35

4 CONCLUSIONS

This study investigated the hydrodynamic performance and biofouling behavior of a cobalt-based ceramic coating compared to Intersleek 1001 antifouling paint through both experimental and computational approaches. The results provide valuable insights into the effectiveness of ceramic coatings in reducing biofouling accumulation and minimizing drag resistance in trawler hulls. Experimental roughness measurements demonstrated that, prior to seawater exposure, the cobalt-based ceramic coating exhibited significantly lower roughness values than Intersleek 1001. However, after 30 days of static seawater exposure, the ceramic coating showed a greater increase in roughness due to biofouling adhesion, with roughness values 23.31% higher than those observed for Intersleek 1001. Despite this, the roughness values obtained for the ceramic coating closely aligned with previous studies, confirming the reproducibility of the experimental findings.

Under dynamic conditions, simulating navigation at 10 knots, the ceramic coating displayed remarkable self-cleaning properties. After 30 days of dynamic testing, its roughness values returned to near-initial conditions, whereas the Intersleek 1001-coated surface retained a significantly higher roughness (1987.10% greater than that of the ceramic coating). These findings suggest that the cobalt-based ceramic coating offers superior biofouling removal capabilities when subjected to hydrodynamic shear stress.

CFD simulations further validated the experimental findings by quantifying the impact of surface roughness on the total drag resistance of a trawler hull. Prior to exposure, the ceramic-coated hull exhibited lower total resistance than the Intersleek 1001-coated hull. After 30 days of static exposure, biofouling-induced roughness increased the total resistance of both coatings; however, dynamic conditions effectively restored the ceramic coating's initial resistance values, whereas the Intersleek 1001-coated hull retained a 6.35% increase in resistance.

Overall, the results highlight the potential of cobalt-based ceramic coatings as a viable alternative to conventional antifouling paints, offering both lower initial roughness and enhanced self-cleaning performance under operational conditions.

ACKNOWLEDGEMENTS

The authors acknowledge Vibrantz Technologies for their invaluable collaboration in the manufacturing of the experimental panels. Their support has been instrumental in making this research possible.

FUNDING

This work was supported by the Government of Cantabria and the European Union Next GenerationEU/PRTR [project Environmentally friendly bioactive coatings for energy improvement and emissions reduction in the fishing shipbuilding industry - BIO-ENER.].

REFERENCES

[1] H. Lindstad, R.M. Bright, A.H. Strømman, Economic savings linked to future Arctic shipping trade are at odds with climate change mitigation, Transp Policy (Oxf) 45 (2016) 24–30. https://doi.org/10.1016/j.tranpol.2015.09.002.

[2] S. García, A. Trueba, D. Boullosa-Falces, H. Islam, C. Guedes Soares, Predicting ship frictional resistance due to biofouling using Reynolds-averaged Navier-Stokes simulations, Applied Ocean Research 101 (2020). https://doi.org/10.1016/j.apor.2020.102203.

[3] L. Trueba-Castaneda, D.S. Sanz, S. Garcia, A. Trueba, Analysis of biofouling economic impact on the Cantabria fishing fleet, in: OCEANS 2021: San Diego – Porto, IEEE, 2021: pp. 1–6. https://doi.org/10.23919/OCEANS44145.2021.9706079.

[4] N. Hadžić, I. Gatin, T. Uroić, V. Ložar, Biofouling dynamic and its impact on ship powering and dry-docking, Ocean Engineering 245 (2022) 110522. https://doi.org/10.1016/j.oceaneng.2022.110522.

[5] D.S. Sanz, S. García, L. Trueba-Castañeda, D. Boullosa-Falces, A. Trueba, Antifouling and Anticorrosive Protection of Renewable Energy Marine Structures with TiO2-Based Enamel, TransNav, the International Journal on Marine Navigation and Safety of Sea Transportation 18 (2024) 419–424. https://doi.org/10.12716/1001.18.02.21.

[6] C.-C. Chang, M.-L. Huang, C.-H. Li, Analysis of emission reduction strategies for the use of alternative fuels and natural carbon sinks in international bulk shipping, Energy Conversion and Management: X 24 (2024) 100702. https://doi.org/10.1016/j.ecmx.2024.100702.

[7] M. Leer-Andersen, L. Larsson, An experimental/numerical approach for evaluating skin friction on full-scale ships with surface roughness, J Mar Sci Technol 8 (2003) 26–36. https://doi.org/10.1007/s10773-003-0150-y.

[8] D.S. Sanz, S. García, A. Trueba, L. Trueba-Castañeda, H. Islam, C. Guedes Soares, D. Boullosa-Falces, Numeric analysis of the biofouling impact on the ship resistance with ceramic coating on the hull, in: Trends in Maritime Technology and Engineering Volume 1, CRC Press, London, 2022: pp. 443–449. https://doi.org/10.1201/9781003320272-49.

[9] Y.K. Demirel, O. Turan, A. Incecik, Predicting the effect of biofouling on ship resistance using CFD, Applied Ocean Research 62 (2017) 100–118. https://doi.org/10.1016/j.apor.2016.12.003.

[10] S. Song, Y.K. Demirel, M. Atlar, An investigation into the effect of biofouling on the ship hydrodynamic characteristics using CFD, Ocean Engineering 175 (2019) 122–137. https://doi.org/10.1016/j.oceaneng.2019.01.056.

[11] D. Owen, Y.K. Demirel, E. Oguz, T. Tezdogan, A. Incecik, Investigating the effect of biofouling on propeller characteristics using CFD, Ocean Engineering 159 (2018) 505–516. https://doi.org/10.1016/j.oceaneng.2018.01.087.

[12] N. Speranza, B. Kidd, M.P. Schultz, I.M. Viola, Modelling of hull roughness, Ocean Engineering 174 (2019) 31–42. https://doi.org/10.1016/j.oceaneng.2019.01.033.

[13] D.S. Sanz, S. García, L. Trueba, A. Trueba, Bioactive Ceramic Coating Solution for Offshore Floating Wind Farms, TransNav, the International Journal on Marine Navigation and Safety of Sea Transportation 15 (2021). https://doi.org/10.12716/1001.15.02.19.

[14] S. García, D. Boullosa-Falces, D.S. Sanz, A. Trueba, M.A. Gomez-Solaetxe, Artificial-intelligence-model to optimize biocide dosing in seawater-cooled industrial process applications considering environmental, technical, energetic, and economic aspects, Biofouling 40 (2024) 366–376. https://doi.org/10.1080/08927014.2024.2363241.

[15] E. Robertson, V. Choudhury, S. Bhushan, D.K. Walters, Validation of OpenFOAM numerical methods and turbulence models for incompressible bluff body flows, Comput Fluids 123 (2015) 122–145. https://doi.org/10.1016/j.compfluid.2015.09.010.

[16] A. Trueba, L.M. Vega, S. García, F.M. Otero, E. Madariaga, Mitigation of marine biofouling on tubes of open rack vaporizers using electromagnetic fields, Water Science and Technology 73 (2016) 1221–1229. https://doi.org/10.2166/wst.2015.597.

[17] D. Boullosa-Falces, D.S. Sanz, S. Garcia, L. Trueba-Castañeda, A. Trueba, Predicting tubular heat exchanger efficiency reduction caused by marine biofilm adhesion using CFD simulations, Biofouling (2022) 1–11. https://doi.org/10.1080/08927014.2022.2110493.

[18] D.S. Sanz, S. García, A. Trueba, H. Islam, C.G. Soares, Prediction of biological development effects on drag forces of ceramic hull coating using Reynolds-averaged Navier–Stokes-based solver, Biofouling (2023) 1–14. https://doi.org/10.1080/08927014.2023.2209020.

[19] A. Trueba, S. García, F.M. Otero, L.M. Vega, E. Madariaga, Influence of flow velocity on biofilm growth in a tubular heat exchanger-condenser cooled by seawater, Biofouling 31 (2015). https://doi.org/10.1080/08927014.2015.1070404.

[20] D.S. Sanz, S. Garcia, A. Trueba, L.M. Vega, L. Trueba-Castaneda, D. Boullosa-Falces, Application of ceramic coatings to minimize the frictional drag penalty on ships, in: OCEANS 2021: San Diego – Porto, IEEE, 2021: pp. 1–5. https://doi.org/10.23919/OCEANS44145.2021.9706045.

[21] D. Boullosa-Falces, S. García, D. Sanz, A. Trueba, M.A. Gomez-Solaetxe, CUSUM chart method for continuous monitoring of antifouling treatment of tubular heat exchangers in open-loop cooling seawater systems, Biofouling 36 (2020) 73–85. https://doi.org/10.1080/08927014.2020.1715954.

[22] D. Boullosa-Falces, M.A. Gomez-Solaetxe, Z. Sanchez Varela, S. García, A. Trueba, D. Sanz, Study of the impact of EMF on the reduction of biofouling in heat exchangers, in: Trends in Maritime Technology and Engineering Volume 1, CRC Press, London, 2022: pp. 511–515. https://doi.org/10.1201/9781003320272-57.

[23] S. Garcia, A. Trueba, L. Vega, E. Madariaga, Improvement of Electromagnetic Fields treatment for biofouling growth control in tubular heat exchanger-condenser cooled by seawater, in: OCEANS 2017 - Aberdeen, IEEE, 2017: pp. 1–5. https://doi.org/10.1109/OCEANSE.2017.8084576.

[24] P. Yi, H. Jia, X. Yang, Y. Fan, S. Xu, J. Li, M. Lv, Y. Chang, Anti-biofouling properties of TiO2 coating with coupled effect of photocatalysis and microstructure, Colloids Surf A Physicochem Eng Asp 656 (2023) 130357. https://doi.org/10.1016/j.colsurfa.2022.130357.
[25] T. Cebeci, P. Bradshaw, Momentum Transfer in Boundary Layers, Hemisphere Publishing Corporation, New York, 1977.
[26] G. Kalitzin, G. Medic, G. Iaccarino, P. Durbin, Near-wall behavior of RANS turbulence models and implications for wall functions, J Comput Phys 204 (2005) 265–291. https://doi.org/10.1016/j.jcp.2004.10.018.
[27] T. Adams, C. Grant, H. Watson, A Simple Algorithm to Relate Measured Surface Roughness to Equivalent Sand-grain Roughness, International Journal of Mechanical Engineering and Mechatronics (2012). https://doi.org/10.11159/ijmem.2012.008.